Journal of Power Sources 194 (2009) 2–9

Contents lists available at ScienceDirect

Journal of Power Sources

journal homepage: www.elsevier.com/locate/jpowsour

Structural and electrical properties of grain boundaries in $Ce_{0.85}Gd_{0.15}O_{1.925}$ solid electrolyte modified by addition of transition metal ions

Wojciech Zając[a,*], Leopoldo Suescun[b], Konrad Świerczek[a], Janina Molenda[a]

[a] AGH University of Science and Technology, Faculty of Materials Science and Ceramics, al. Mickiewicza 30, 30-059 Kraków, Poland
[b] Cryssmat-Lab/Detema, Facultad de Química, Universidad de la República, P.O. Box 1157, Montevideo, Uruguay

ARTICLE INFO

Article history:
Received 17 October 2008
Received in revised form 4 December 2008
Accepted 5 December 2008
Available online 11 December 2008

Keywords:
Ceria
Solid oxide fuel cell
Transition metals
Grain boundaries
Synchrotron X-ray powder diffraction studies
Impedance spectroscopy

ABSTRACT

In this work we present studies on applicability of transition metal additives as sintering and electrical conductivity aids for cerium gadolinium oxide electrolyte. The nanosized $Ce_{0.85}Gd_{0.15}O_{1.925}$ powder obtained by coprecipitation method was modified with Cr^{3+}, Fe^{3+}, Ni^{2+} or Cu^{2+} ions. Using high-intensity high-resolution X-ray powder diffraction data we have determined that Cr, Fe and Ni ions do not incorporate into the cerium gadolinium oxide surface or bulk when sintered at 1300 °C, but react with Gd ions to form $Cr_{0.9}Gd_{0.1}O$, $GdFeO_3$ and $GdNiO_3$ phases, while Cu incorporates in the material up to 0.7 mol% with a significant fraction of remaining material showing poorly crystalline CuO phase. The nanosized $Ce_{0.85}Gd_{0.15}O_{1.925}$ material shows already improved sintering properties than previous reports but full sintering is not achieved below 1300 °C, however Cr, Fe and mainly Cu impregnation allows full sintering at 1300 °C. 0.5 mol% Ni impregnated material sintered at 1500 °C shows enhanced grain boundary conductivity that probably indicates that Ni incorporates into $Ce_{0.84}Gd_{0.15}O_{1.925}$ above 1300 °C. The global results indicate, however, that optimization of ceria microstructure is at least of equal importance for sinterability and grain boundary conductivity than impregnation of the material with transition metal ions.

1. Introduction

One of the most important issues for the progress of the Solid Oxide Fuel Cells (SOFC) technology is to develop a solid electrolyte material with higher oxygen ion conductivity in comparison with currently used materials. $Ce_{1-x}Gd_xO_{2-x/2}$-based electrolytes seem to be promising candidates for application in SOFC, especially in the intermediate temperature range (cells working at 600–800 °C) [1–4]. The amount of gadolinium ions, which substitute cerium cations in their crystallographic positions, plays a significant role in terms of optimization of the ionic conductivity, with compositions between 10 and 20 mol% being the optimal [5]. Since further optimization of the electrical conductivity of grain interior for ceria-based electrolyte material seems very hard to achieve [6], other ways to lower the resistivity of the electrolyte material should be found.

As for most of polycrystalline ceramics, also for ceria-based electrolyte, the overall physicochemical properties are determined by both bulk lattice and grain boundary features. In terms of the ionic conductivity a deteriorating effect of grain boundaries has been observed for both zirconia [7] and ceria electrolytes [2], what limits the total conductivity of the electrolyte to that of the grain boundary. Especially unfavourable influence on the grain boundary properties of ZrO_2- and CeO_2-based materials has been ascribed to a presence of SiO_2 impurities, which forms amorphous, siliceous layers showing a blocking effect for oxygen ion conductivity. Nevertheless, also for high-purity Gd-doped ceria, inferior conductivity of grain boundaries in relation to bulk has been observed. This was attributed to the space charge effect [8–10], which leads to a decreased concentration of oxygen vacancies in the grain surface and, as a consequence, to a decreased ionic conductivity. Taking this into account an effort leading to an improvement of the grain boundary ionic conductivity is necessary.

To overcome this drawback the addition of a small amount of transition metal ions in the surface was proposed [11–15]. According to previous papers, transition metal ions, which mostly locate at the grain boundary region or at triple point junctions between grains of the sinter [11] can act as both scavengers for siliceous layers and alternators for the space charge potential. Previous works were focused mainly on an addition of Mn^{4+}, Fe^{3+}, Co^{2+} and Cu^{2+}. Among them Fe^{3+} and Co^{2+} showed the strongest profitable effect on the grain boundary conductivity. Moreover, all of these additives are beneficial in terms of sinterability [13,14,16], which is apparently due to the emergence of a viscous flow sintering.

Another motivation of these studies was the fact that in a fuel cell the electrolyte works in a vicinity of other parts of the fuel

* Corresponding author. Tel.: +48 126172026; fax: +48 126172522.
E-mail address: wojciech.zajac@agh.edu.pl (W. Zając).

0378-7753/$ – see front matter © 2008 Elsevier B.V. All rights reserved.
doi:10.1016/j.jpowsour.2008.12.020

cell: perovskite type cathode (usually containing some of Mn, Fe, Co and/or Ni ions), anode (containing Ni) and/or an interconnector – metallic or ceramic (containing Fe, Cr, etc.) [3,17] that, at higher temperatures, may lead to an uncontrolled contamination of the solid electrolyte, due to chemical reactivity between cell components. So it is required to know the effect of such a process on the conductivity of the electrolyte.

The aim of this work was to investigate the relation between the sintering temperature, structure and electrical conductivity of $Ce_{0.85}Gd_{0.15}O_{1.925}$ electrolyte modified with addition of transition metal ions: Cr^{3+}, Fe^{3+}, Ni^{2+} and Cu^{2+}.

The ceria electrolyte with composition $Ce_{0.85}Gd_{0.15}O_{1.925}$ was chosen as a starting point for this study. Four different transition metal additives (Cr, Fe, Ni and Cu) with three concentrations each (0.5, 1.0 and 2.0 mol%) were selected to be investigated.

2. Experimental

$Ce_{0.85}Gd_{0.15}O_{1.925}$ (abbreviated in this work as CGO15) powder was obtained by a coprecipitation method. A solution of standard purity cerium(III) and gadolinium nitrates ($Ce(NO_3)_3{\cdot}6H_2O$, >99%, Fluka; $Gd(NO_3)_3{\cdot}6H_2O$, 99.9%, Aldrich) with appropriate molar ratio and total concentration of cations equal to 0.1 mol dm^{-3} was added to an aqueous solution of ammonia (~6 wt.%) during intensive mixing. Obtained precipitate was washed with distilled water and isopropyl alcohol, filtered, dried and calcined at 500 °C for 1 h. Afterwards, an aqueous solution of transition metal nitrates ($Cr(NO_3)_3{\cdot}9H_2O$, >99.9%, POCH; $Fe(NO_3)_3{\cdot}9H_2O$, >99%, POCH; $Ni(NO_3)_2{\cdot}6H_2O$, 99%, Chempur; $Cu(NO_3)_2{\cdot}3H_2O$, >99%, Chempur) was added to CGO15 powder, what gave a suspension. Next, the suspension was dried at 70 °C and calcined again at 500 °C for 1 h in order to decompose incorporated transition metal nitrates. Such obtained powders were formed into 13 mm pellets, about 2 mm thick, using uniaxial pressing under pressure of 70 MPa followed by an isostatic pressing under 200 MPa of pressure.

Uniaxial dilatometric curves were measured during sintering in a Linseis L75/043B dilatometer up to 1300 °C using a constant heating rate of 1 deg min^{-1}. Obtained results were corrected taking into account thermal expansion of the empty dilatometer. Samples for electrical measurements were sintered at 1300 and at 1500 °C applying the same heating rate as in dilatometric measurements.

Conventional X-ray powder diffraction (XRD) measurements of unmodified CGO15 powder after calcination at 500 °C were performed using a Philips X'Pert Pro diffractometer with Cu K_α radiation. Surface area of CGO15 powder was measured by means of BET method using Sorpty 1750 equipment. The phase composition of the samples sintered at 1300 °C was investigated using synchrotron X-ray powder diffraction (SXRD) at Argonne's Advanced Photon Source, 11BM-B beamline [18]. The samples were loaded in 1 mm kapton capillaries for a transmission geometry experiment using ~30 keV energy radiation (λ = 0.41425 Å). Data was collected using the 12 detector high-resolution high-intensity setup where each detector scans different ranges of the pattern and the contribution of each detector is averaged to form the final dataset in the $5 \leq 2\theta \leq 50$ deg range with a step of 0.001 deg and data collection of 0.1 s/step. Fits of the diffraction data were performed by the Rietveld method with the GSAS/EXPGUI suite of programs [19,20]. Background, profile and symmetry allowed structural parameters were simultaneously refined for $Ce_{0.85}Gd_{0.15}O_{1.925}$ or its Gd-depleted derivatives and the secondary transition metal containing phase. Absorption correction was performed assuming 40% packing density of the sample in the capillary.

The electrical conductivity of the sintered samples was measured using an impedance spectroscopy Solartron 1260 frequency response analyser with an excitation voltage of 0.2 V. Data were collected in the 0.1 Hz–10 MHz frequency range, every 50 °C from 300 to 700 °C. Before the measurement both sides of the samples were polished and covered with platinum paste (ITME, type P-321) to provide an electrical contact. Registered impedance spectra were analyzed using ZView® software from Scribner Associates.

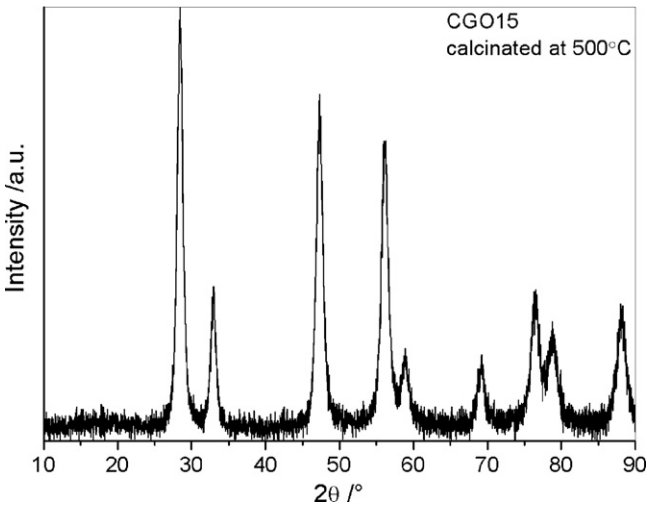

Fig. 1. XRD pattern for CGO15 nanosized powder after calcination at 500 °C.

3. Results and discussion

3.1. Structural characterization of starting CGO15

XRD measurements showed that the unmodified CGO15 powder after calcination at 500 °C was a single-phase, fluorite-type material (Fig. 1).

Large peak broadening was observed as expected for a very small crystallite size of the starting material. According to the Scherrer equation, the crystallite diameter was estimated to be close to 10 nm. This value corresponds well to the particle diameter obtained from BET surface area measurements. The specific surface area was measured to be 72 m^2 g^{-1}, corresponding to an average particle diameter of 11 nm. Good agreement between XRD and BET data indicates that none or only little agglomeration of the primary crystallites takes place during the first steps of processing. This is favourable to obtain uniform starting distribution of transition metal ions after the impregnation step as the solution may reach all grain surfaces.

3.2. Sintering

Sinterability of the obtained powders was tested using the uniaxial dilatometry method. Fig. 2a–d depict linear shrinkage rate calculated as the numerical derivative of the temperature dependence of the relative length change for unmodified CGO15 and for Cr, Fe, Ni and Cu-containing pellets.

In the case of CGO15 (solid line in Fig. 2a–d) sintering starts between 500 and 600 °C, whereas maximum shrinkage rate appears between 650 and 850 °C. One may distinguish two overlapping shrinkage maxima (at about 700 and 800 °C) which may arise from slightly two-modal distribution of grain-sizes in prepared powder, above 1000 °C shrinkage rate slows down, but even up to 1300 °C is not counterbalanced by the thermal expansion of the material. Such sintered pellets had relative density of 98%. To our best knowledge this result is one of the best in the literature and suggests that by appropriate preparation procedure one may obtain CGO powders with highly enhanced sinterability.

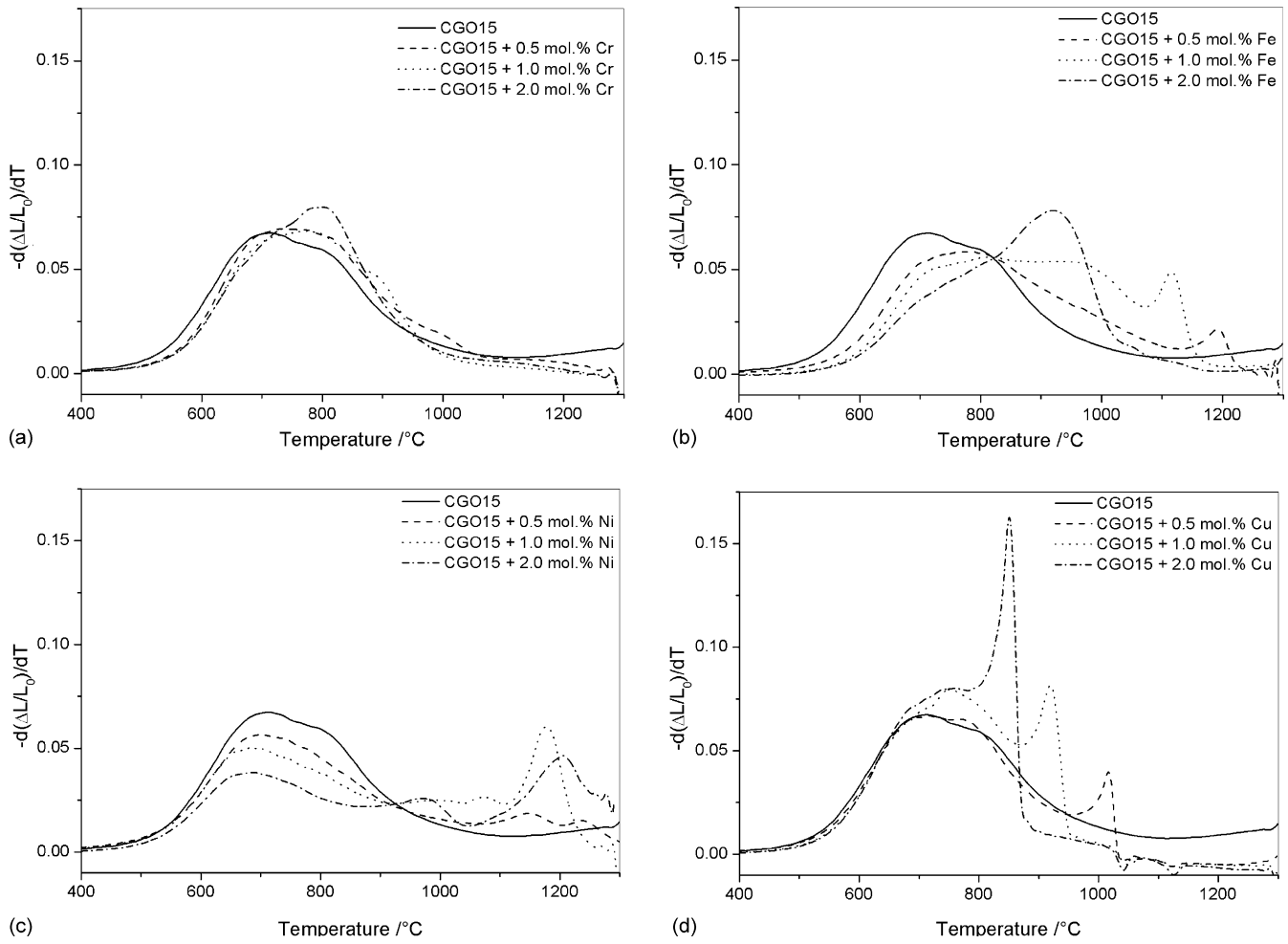

Fig. 2. Shrinkage rate vs. temperature for (a) CGO15 + Cr; (b) CGO15 + Fe; (c) CGO15 + Ni and (d) CGO15 + Cu.

The presence of transition metal ions in the sintered CGO pellets led to a significant change of the sintering behaviour. New maxima appeared above 800 °C in all the cases (Fig. 2a–d), though their intensity vary for different ions. The observed shrinkage maxima presumably correspond to a viscous flow sintering, arising from a low melting temperature of a mixture formed by cerium, gadolinium, 3*d* ions and other impurities in the grain boundary region. The temperature of the new maxima and their intensity correlates with the amount of the additive, what is the clearest in the case of Fe and Cu. In the case of Ni, the dependence seems to be more complicated, which may be related to the possible chemical instability of formed reaction compounds (see Section 3.3 and Section 3.4 below). The most intense effect was observed in the case of Cu ions, whereas the least effect was registered for Cr ions. Contrary to the unmodified CGO15, for samples containing transition metal ions, at temperatures above the maximum, the shrinkage stopped and an expansion could be observed. This most likely is related to the thermal expansion and implies that the process of sintering was ended. The relative density (measured by Archimedes method) of all obtained samples was in the range of 95–97% regardless to type of transition metal ion and its concentration. This observation may be rationalized taking into account favourably low sintering temperature of unmodified CGO15 powder itself in comparison with the literature data. Values of the temperature of maximum sintering rate reported in the literature for CGO vary in a wide range depending mainly on the grain size of the starting powder. To illustrate this phenomenon a few results have been gathered in Table 1 in comparison with ours. It is worth mentioning that the effect of transition metal ions on sintering is most remarkable for micrometer-grain-sized powder or for powder with strong agglomeration. In this case the sintering temperature of the unmodified powder is usually above 1000 °C and the addition of transition metal ions provides the

Table 1
Temperature of the maximum shrinkage rate.

Composition	Particle size (nm)	Temperature of maximum shrinkage rate (°C)		Ref.
		Pure CGO	After modification	
CGO20 + 0.5 at.% Fe	100–500	1520	1335	[12]
CGO10 + 5 mol% Li	40 (75 × 600 nm agglomerates)	1000	750	[16]
CGO20 + 2 mol% Co	20	930	870	[14]
CGO15 + 2 mol% Cr	10	700–800	800	This work
CGO15 + 2 mol% Fe	10	700–800	920	This work
CGO15 + 1 mol% Ni	10	700–800	1177	This work
CGO15 + 2 mol% Cu	10	700–800	850	This work

lowering of the sintering temperature of up to 200 °C. However, in the case of nanometer-size powder, as it is shown in this work, the sintering temperature is especially low, even for unmodified CGO, and the addition of transition metal ions does not lead to a further decrease of this temperature. It allows, however, in the case of Cu addition to achieve full sintering well below 1300 °C.

On the basis of these results two sintering temperatures were selected for preparation of samples for further testing: 1300 °C, which allows obtaining sinters with density high enough to be gas-tight, and could serve as an electrolyte membrane, and 1500 °C, which is more common in the literature.

3.3. Phase composition

The phase composition of all obtained samples were studied by XRD method, however samples sintered at 1300 °C were tested with special care using SXRD, since their electrical properties seem to be, to some extent, different from previously reported ones.

Conventional XRD measurements for all samples sintered either at 1300 or 1500 °C showed they are composed of single-phase fluorite-type crystal structure and no trace of additional phases could be detected in such measurements. While SXRD pattern for unmodified CGO15 (shown in Fig. 3) revealed high purity of the material, patterns for materials with addition of transition metal ions (Fig. 4a–d) indicate that incorporated transition metal ions form new crystal phases and do not exist as amorphous layers around CGO15 grains. Presumably, these new crystal phases are located at triple point junctions as seen by Avila-Paredes and Kim using TEM [11].

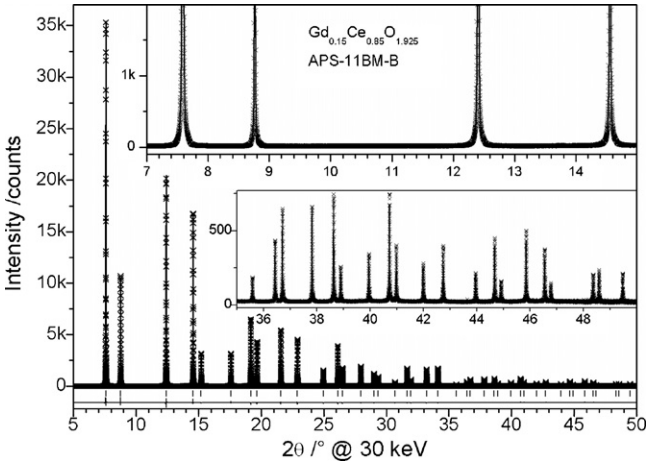

Fig. 3. Rietveld fit of synchrotron X-ray powder diffraction pattern collected for CGO15 sintered at 1300 °C (× symbols represent observed points, line through points is calculated intensity, | marks indicate reflection positions and bottom line the difference between observed and calculated intensities).

For chromium, the formation of a very rare halite-type CrO phase partially doped with Gd with approximate composition $Gd_{0.1}Cr_{0.9}O_{1-\delta}$ (Gd content refined for 2 mol% doping) was detected,

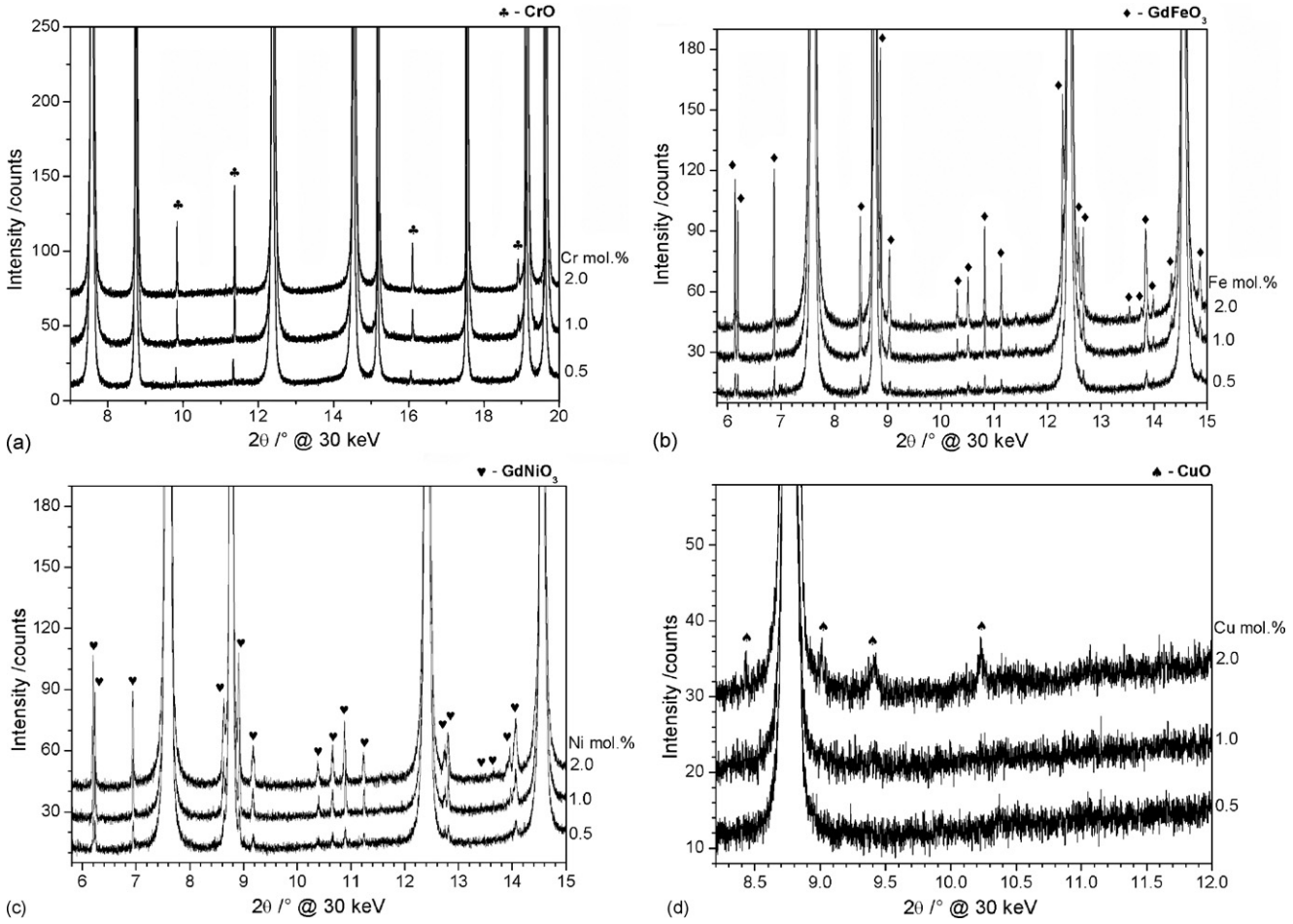

Fig. 4. Synchrotron X-ray powder diffraction patterns for CGO15 modified with of (a) Cr; (b) Fe; (c) Ni and (d) Cu. The intensity scale in the left corresponds to the intensity of the lowest pattern, other patterns were shifted to allow visualization of peaks. Note that the y scale for Cu is much shorter than for other TMs to improve visualization of very small CuO peaks.

Table 2
Goodness of fit parameters for Rietveld fit of the synchrotron X-ray powder diffraction patterns for the samples sintered at 1300 °C.

Composition	χ^2	wR_p (%)	R_p (%)
CGO15	2.494	6.03	4.38
CGO15 + 0.5Cr	2.814	7.74	5.63
CGO15 + 1.0Cr	2.976	6.95	5.01
CGO15 + 2.0Cr	2.409	6.98	5.40
CGO15 + 0.5Fe	2.008	6.70	5.06
CGO15 + 1.0Fe	2.867	7.02	5.16
CGO15 + 2.0Fe	3.013	6.98	5.36
CGO15 + 0.5Ni	3.103	7.28	5.60
CGO15 + 1.0Ni	3.238	7.17	5.35
CGO15 + 2.0Ni	4.290	8.17	6.60
CGO15 + 0.5Cu	2.920	7.20	5.42
CGO15 + 1.0Cu	2.700	7.34	5.57
CGO15 + 2.0Cu	4.331	8.07	5.74

whereas addition of Fe and Ni led to the formation of perovskite-type phases with compositions of $GdFeO_3$ and $GdNiO_3$, respectively. Only Cu addition produced no reaction with Gd but led to the formation of a very small amount of CuO phase. The χ^2, R_p and wR_p values for the Rietveld fits of the obtained patterns are shown in Table 2.

The formation of halite and perovskite-type phases lead to a lowered gadolinium content in the main fluorite phase and as a consequence influences bulk as well as grain boundary properties. Fig. 5 presents refined content of transition metal ions secondary phase vs. transition metal ions content as used in the synthesis procedure, whereas Fig. 6 shows CGO15 cell volume vs. the additive content.

In the case of perovskite phases the refined content reproduces very closely the amount of transition metal ions used during the synthesis, indicating that detected perovskite phase gathers the whole amount of iron and nickel. The presence of heavy Gd cations in CrO phase is proposed after an undoped CrO phase would not explain the higher than expected weight percentage of this secondary phase. Refinement of Gd/Cr ratio in $Gd_{0.1}Cr_{0.9}O_{1-\delta}$ is complicated due to the very small amount of this phase in the studied samples and the Gd content may differ by up to 30% of the reported value. The accurate refinement of the amount of this phase (Fig. 5a) suggests that the reported value is reasonable within the precision of the study.

The opposite effect was observed for Cu ions. For sample containing 0.5 mol% of Cu no new peaks were detected, while for 1.0 and 2.0 mol% hardly visible peaks corresponding to CuO appeared and allowed to calculate the CuO content equal to 0.03 and 0.12 mol%, respectively. Such a small content of the new phase, in relation to amount introduced during synthesis, demonstrates that some Cu dissolves in ceria lattice forming a solid solution. We have estimated a limit of the solid solution formation in the CGO—Cu system to be 0.7 mol% (Fig. 5b) by extrapolation of observed contents in 1 and 2 mol% samples. But the slope of the dependence of the refined Cu content vs. Cu amount used during synthesis is less steep than the one expected for complete segregation of a crystalline CuO phase. This may suggest the existence of some amount of an amorphous phase present in the samples, probably at CGO grain boundaries.

CGO15 unit cell volume changes follow the expected trend with increasing amount of transition metal content. In the case of iron and nickel, formation of gadolinium containing perovskite phases was accompanied by relatively strong decrease of the lattice dimensions of remaining CGO phase as shown in Fig. 6. This effect is connected with decreased gadolinium content in ceria and it stays in an agreement with the data of $Ce_{1-x}Gd_xO_{2-x/2}$ unit cell volume as a function of gadolinium content [21]. A deviation from the expected linear behaviour for Ni-containing samples, specifically for 2 mol%, may be explained by the observation of peak

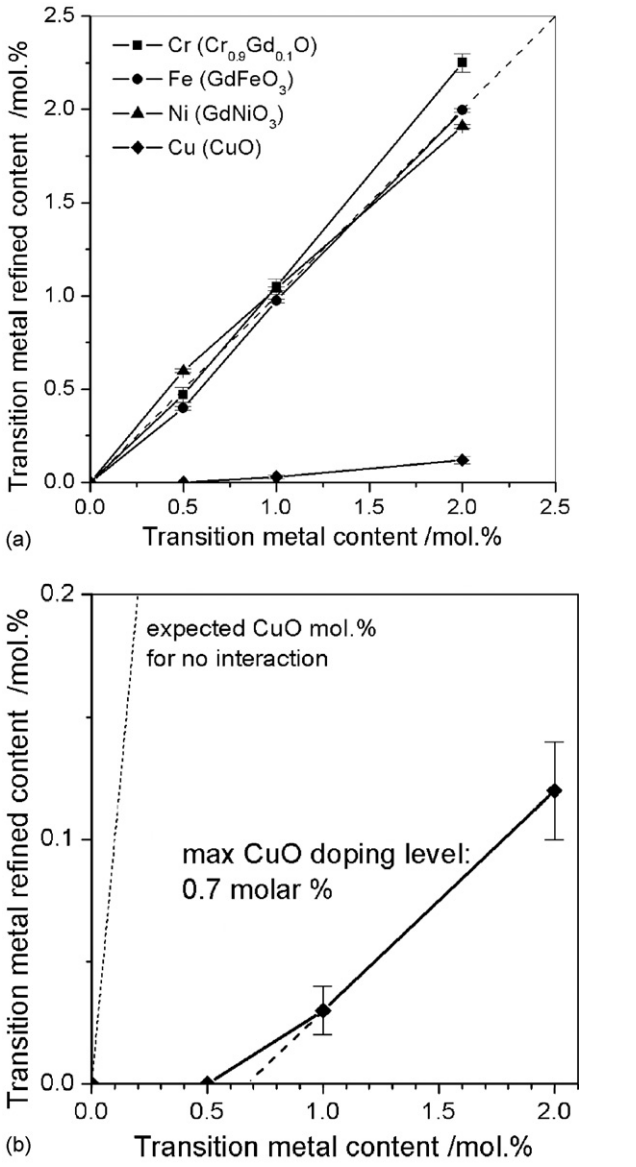

Fig. 5. (a) Refined content of transition metal containing phase vs. transition metal content used during synthesis and (b) refined Cu content of vs. Cu amount used during synthesis. Dash line indicates 1:1 correspondence between calculated and found concentrations.

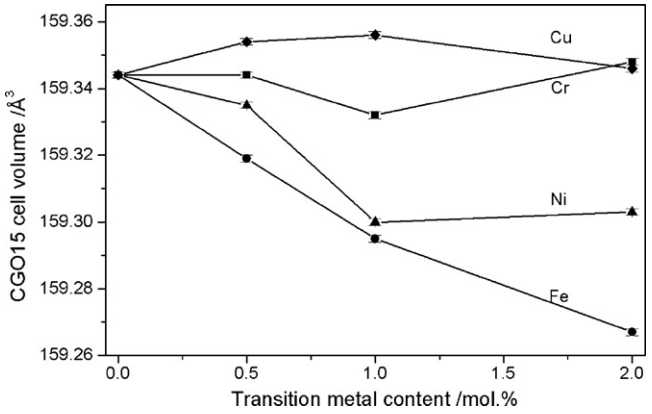

Fig. 6. $Ce_{1-x}Gd_xO_{2-x/2}$ unit cell volume vs. transition metal content. Gd content is significantly reduced by Fe or Ni molar content for the different samples.

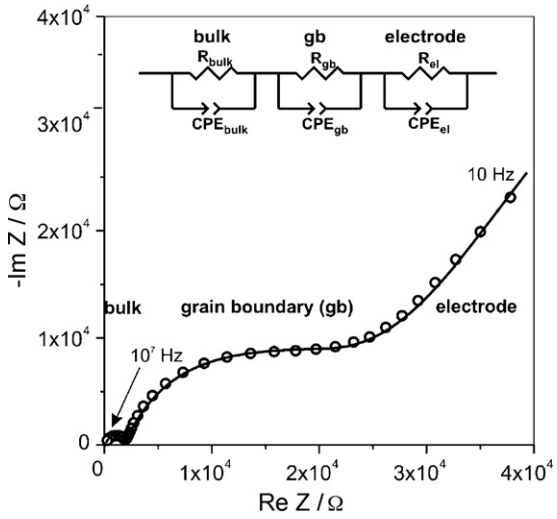

Fig. 7. Impedance spectrum of CGO15 at 358 °C (circles – experimental data; solid line – simulation) and the equivalent circuit used for interpretation of impedance data.

shape changes in CGO15 material between 1 and 2 mol% patterns that reduced the quality of the fit in the second case (see Table 2). These changes may be associated to an ongoing transformation of the sample at 1300 °C as depicted in dilatometry measurements for Ni 2 mol% sample (Fig. 2c) where the largest magnitude of volume change is observed for this sample respect to all the other studied ones. This is also consistent with the observation of broad peaks of $GdNiO_3$ as compared with $GdFeO_3$ in Fig. 4b and c. As expected the presence of Cr and Cu ions caused only small variations in lattice constants that can be considered to fall within the experimental error.

3.4. Electrical conductivity

Fig. 7 shows an exemplary impedance spectrum for CGO15 measured at 358 °C, at which three separate semicircles may be distinguished. The lowest frequency semicircle is attributed to the sample-electrode connection; the medium frequency semicircle corresponds to grain boundaries, while the highest frequency arc is attributed to the grain interior (bulk) response. This type of spectrum is usually modelled as three RC (or often RCPE) elements connected in series (as it is presented in Fig. 7) [1]. The separation of these three contributions takes place due to different time constants (*RC*, where *R* – resistance, *C* – capacitance). In the present case the capacitances of the components at 358 °C (calculated from fitting the experimental data) were $C_{bulk} = 10^{-11}$ F, $C_{gb} = 10^{-8}$ F and $C_{el} = 10^{-7}$ F, in good agreement with values estimated by Pérez-Coll et al. [22]. The observed semicircles were slightly depressed, probably due to some dispersion of physical properties. This lack of homogeneity is described with parameter *n*, which for ideal capacitor equals 1. For the measured spectra, *n* was 0.8 for bulk and 0.7 for both grain boundary and electrode response. The time constants of semicircles changed with temperature and, as a consequence, the observed semicircles shifted to higher frequencies as temperature rose. Analysis of the impedance spectra measured as a function of temperature allowed to plot Arrhenius dependences of the bulk and grain boundary electrical conductivities of the considered materials.

Fig. 8a and b present these contributions to the total electrical conductivity for CGO15 sintered at 1300 and 1500 °C. In the case of the material sintered at 1500 °C (Fig. 8b) for the whole examined temperature range the bulk conductivity is higher than the grain boundary one. The difference is about 2.6 orders of magnitude at 300 °C and 0.3 orders of magnitude at 700 °C. This causes that the total conductivity is mainly affected by the grain boundary contribution. Somewhat different situation takes place for CGO15 sintered at 1300 °C (Fig. 8a). Here the bulk and grain boundary conductivities are closer and whereas at 300 °C the bulk conductivity is about 0.6 orders of magnitude higher than the grain boundary one, at 700 °C the situation is reversed and the grain boundary conductivity is about 0.3 orders of magnitude larger than the bulk. It should be pointed out that, for both sintering temperatures, bulk conductivity remains almost unchanged, except of a little difference in activation energies. The reason of the difference in electrical properties between CGO15 sintered at 1300 °C and 1500 °C is probably related to changes in the composition of grain boundary phase caused by an intensification of segregation of impurities present in the material and/or other microstructural changes such as crystal growth. The segregation is, most probably, more intensive during sintering at higher temperatures which results in deteriorated conductivity. Similar, but not so large, effect of sintering temperature on the grain boundary conductivity was observed by Zhang et al. [23]. Comparing previously published data of the electrical conductivity of CGO15 [2,24] and the values obtained in this work one may conclude that the reported bulk conductivities are very

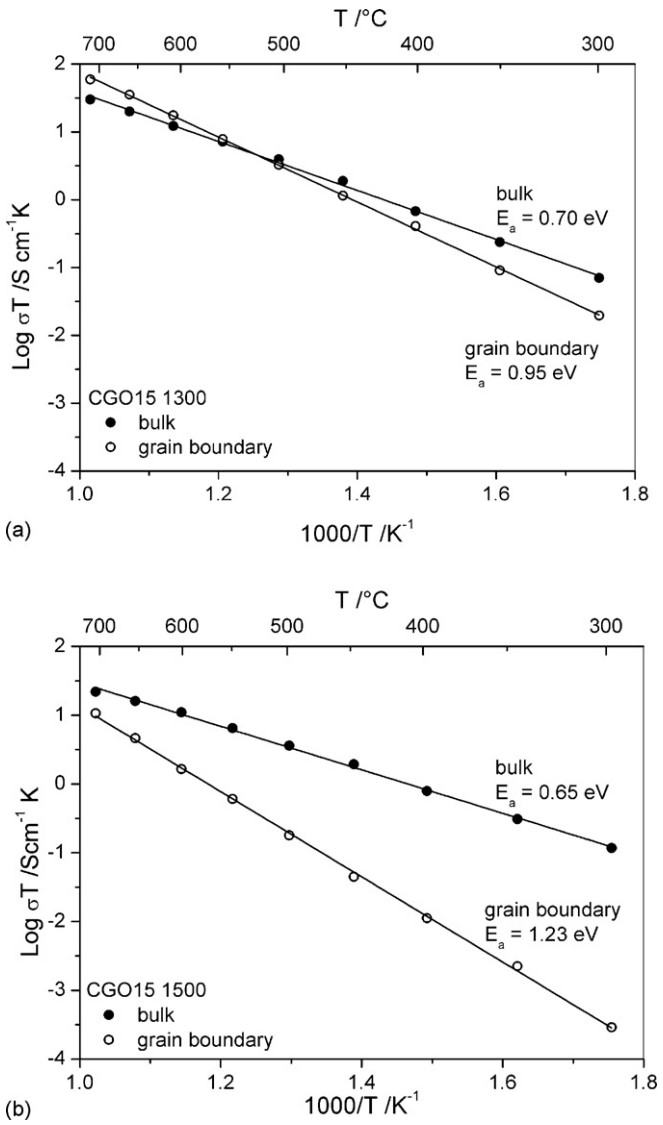

Fig. 8. Electrical conductivity of bulk and grain boundary vs. temperature for CGO15 sintered at (a) 1300 °C and (b) 1500 °C.

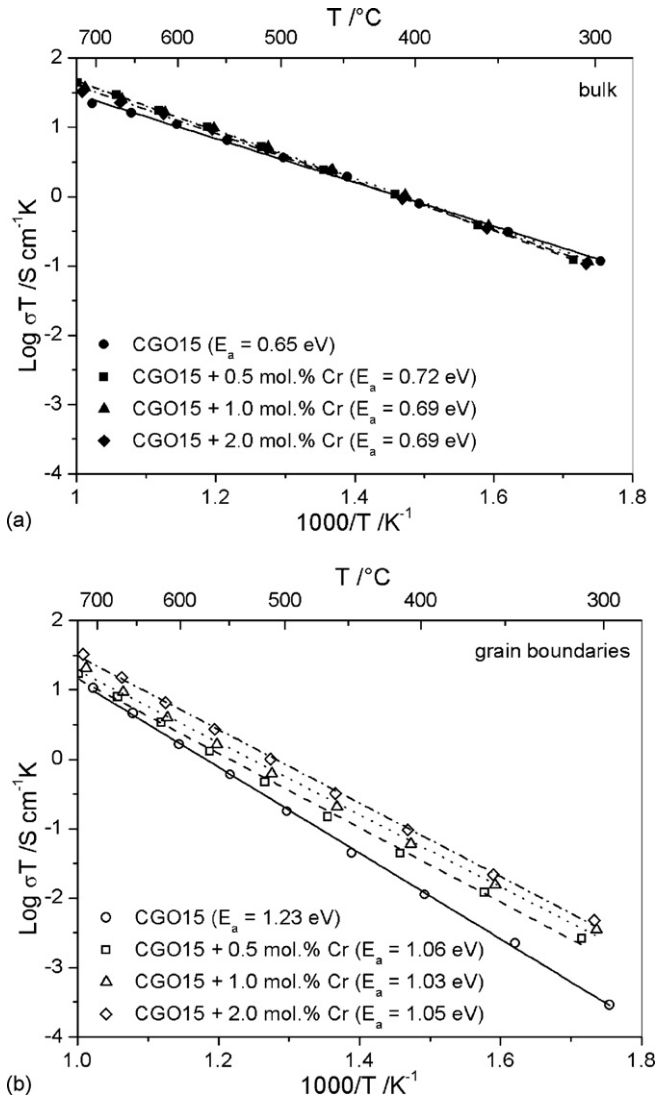

Fig. 9. The influence of chromium on (a) bulk and (b) grain boundary electrical conductivity of CGO15 sintered at 1500 °C.

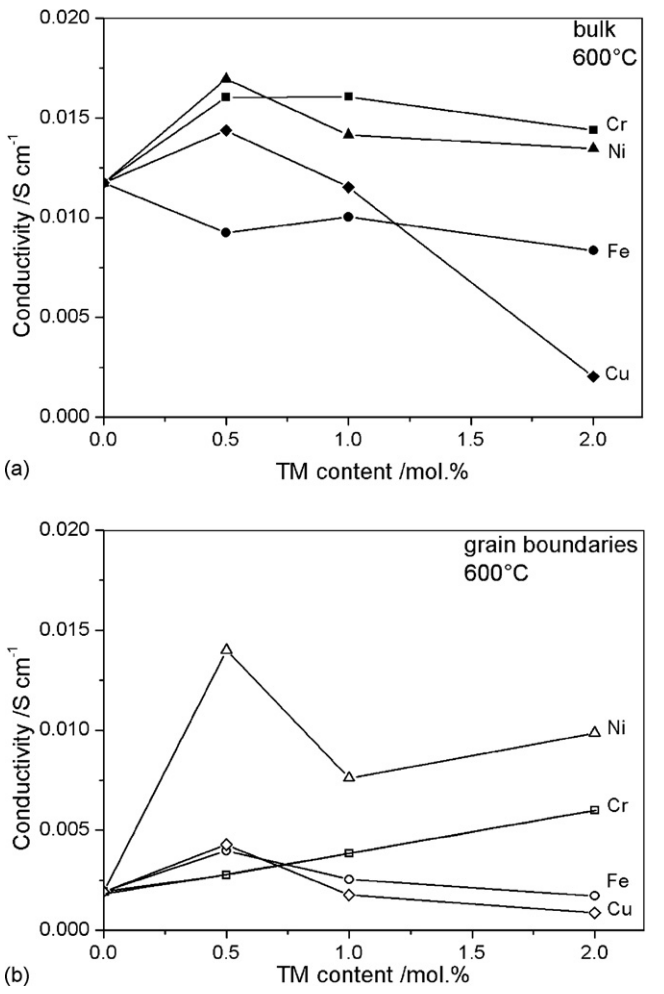

Fig. 10. Electrical conductivity of CGO15 vs. transition metal ions content sintered at 1500 °C.

similar. However, grain boundary conductivity is very sensitive to impurities present in the materials and also depends on preparation conditions. This leads to a discrepancy between different communications. Our results for grain boundary electrical conductivities for CGO15 sintered at 1300 °C lay in the middle of the range, whereas for samples sintered at 1500 °C seems to be rather small.

The observed major improvement of the electrical conductivity of CGO15 sintered at 1300 °C comparing to the sample sintered at 1500 °C is of the same order of magnitude as the improvement achieved by transition metal modification reported in literature. Therefore, the difference of the CGO15 grain boundary electrical conductivity for two applied sintering temperatures led to the difference in the effect of transition metal ions addition.

As an example Fig. 9a and b depict the bulk and grain boundary electrical conductivities for CGO15 sintered at 1500 °C in the case of chromium addition. In this case the influence of transition metal additive on bulk conductivity is minor (Fig. 9a), while the effect on grain boundaries is much intensive. The results for all tested compositions sintered at 1500 °C were gathered in Fig. 10a and b, where the electrical conductivity vs. transition metal ions content is presented. In the case of all tested materials effect of 3*d* metal addition on the bulk conductivity changes was minor and did not exceed ±50%, except CGO15 + 2.0 mol% Cu where a solid solution formation is postulated, that leads to a decreased electrical conductivity. Changes of the grain boundary electrical conductivity upon transition metal ions introduction was much more significant. For example in the case of CGO15 + 2.0 mol% Ni six-fold improvement was achieved.

Similarly as for unmodified CGO15, also for transition metal ions containing materials the improvement of the grain boundary conductivity was observed upon lowering the sintering temperature. However, in this case the improvement was not so significant and as a consequence it was possible to achieve only slight improvement only for 1.0 and 2.0 mol% of Fe ions. The electrical conductivity values measured at 600 °C for prepared compositions were collected in Table 3.

As can be seen analysing data from Table 3 the actual effect of transition metal ions addition cannot be easily described, especially for the materials sintered at 1300 °C where clear segregation of phases is observed for Cr, Fe and Ni impregnated samples. It seems that the starting properties of the unmodified CGO play an extremely important role and optimization of the pure CGO has similar effect as transition metal ions addition. For the materials sintered at 1300 °C, with an exception of: CGO15 + 1.0 and 2.0 mol% Fe and 2.0 mol% Ni, the improvement of the electrical conductivity upon transition metal ions addition was not observed. Correlating this fact with structural analysis presented in part 3.3, which showed the presence of crystal phases of crystallite sizes of the order of micrometers, one may come to conclusion that the interaction of transition metal ions with CGO15 is rather subtle. Probably

Table 3
Bulk and grain boundary electrical conductivity of CGO15 with addition of transition metal ions sintered at 1300 and 1500 °C. Electrical conductivity higher than for unmodified CGO15 were marked with gray colour. The maximum relative error of the presented values equals about 15%.

Composition	σ_{bulk} at 600°C/mS cm^{-1}		σ_{gb} at 600°C/mS cm^{-1}	
	Sintered at 1300°C	Sintered at 1500°C	Sintered at 1300°C	Sintered at 1500°C
CGO15	13.1	11.7	17.5	1.9
CGO15+0.5Cr	8.4	16.1	7.9	2.8
CGO15+1.0Cr	7.6	16.1	6.1	3.8
CGO15+2.0Cr	4.8	14.4	2.2	6.0
CGO15+0.5Fe	8.0	9.3	8.3	4.0
CGO15+1.0Fe	17.2	10.0	19.4	2.5
CGO15+2.0Fe	17.2	8.4	17.5	1.7
CGO15+0.5Ni	6.7	17.0	3.8	14.0
CGO15+1.0Ni	6.8	14.2	2.8	7.6
CGO15+2.0Ni	14.6	13.5	17.0	9.9
CGO15+0.5Cu	11.2	14.4	5.4	4.3
CGO15+1.0Cu	8.1	11.5	2.6	1.8
CGO15+2.0Cu	5.8	2.0	3.0	0.9

these secondary phases occupy triple point junctions, what causes that the only mechanism of interaction may be through gadolinium extraction (at least for Fe, and Ni), where perovskite phases were formed.

However for CGO15 sintered at 1500 °C, which had lower electrical conductivity than the one from 1300 °C, the addition of transition metal ions seems to be beneficial, what stays in agreement with literature data [11,12]. This observation may be rationalized assuming decomposition at temperatures above 1300 °C of formed perovskites and/or possible wetting of grain boundaries by the transition metal ions which would alternate the space charge potential. The first hypothesis could also be confirmed by thermal expansion measurements that clearly show that for 2 mol% Ni sample there is some kind of process still occurring at 1300 °C.

It should be noted however, that the most of obtained materials posses sufficiently high electrical conductivity for practical application for instance for SOFCs working at intermediate temperature range.

Further high-intensity high-resolution X-ray diffraction measurements will be performed to determine the difference between samples sintered at 1300 and 1500 °C.

4. Conclusions

This work shows, to the best of our knowledge for the first time, that crystalline phases are formed upon the addition of a small (less than 2 mol%) amount of transition metal (Cr, Fe, Ni and Cu) ions to CGO15 material, to modify ceria grain boundaries.

Performed studies revealed that in the case of not optimized (sintered at 1500 °C) electrolyte materials the improvement of the ionic conductivity upon the addition may be significant, however appropriate type and amount of 3*d* metal is required. The applicability of transition metal additives for ceria-based electrolytes for which target sintering temperature is around 1300 °C is doubtful. Our studies revealed that regarding sinterability and grain boundary conductivity the optimization of the microstructure of starting ceria material is at least of equal importance to the impregnation of grain boundaries with transition metal ions.

Acknowledgement

This work was supported by Polish Ministry of Science and Higher Education under grant N N507 4441 33.

The authors are indebted to B.H. Toby and J. Doebbler for their assistance with synchrotron data collection and processing.

Use of the Advanced Photon Source at Argonne National Laboratory was supported by the U.S. Department of Energy, Office of Science, Office of Basic Energy Sciences, under Contract No. DE-AC02-06CH11357.

The authors would like to gratefully thank Prof. Bogdan Dabrowski for fruitful discussions.

References

[1] H. Inaba, H. Tagawa, Solid State Ionics 83 (1996) 1–16.
[2] B.C.H. Steele, Solid State Ionics 129 (2000) 95–110.
[3] S.M. Haile, Acta Mater. 51 (2003) 5981–6000.
[4] J. Molenda, K. Świerczek, W. Zając, J. Power Sources 173 (2007) 657–670.
[5] K. Eguchi, T. Setoguchi, T. Inoue, H. Arai, Solid State Ionics 52 (1992) 165–172.
[6] W. Zając, J. Molenda, Solid State Ionics 179 (2008) 154–158.
[7] M. Aoki, Y.-M. Chiang, I. Kosacki, L.J.R. Lee, H. Tuller, Y. Liu, J. Am. Ceram. Soc. 79 (1996) 1169–1180.
[8] X. Guo, R. Waser, Prog. Mater. Sci. 51 (2006) 151–210.
[9] T.S. Zhang, J. Ma, H. Cheng, S.H. Chan, Mat. Res. Bull. 41 (2006) 563–568.
[10] X. Guo, W. Sigle, J. Maier, J. Am. Ceram. Soc. 86 (2003) 77–87.
[11] H.J. Avila-Paredes, S. Kim, Solid State Ionics 177 (2006) 3075–3080.
[12] T.S. Zhang, J. Ma, L.B. Kong, S.H. Chan, P. Hing, J.A. Kilner, Solid State Ionics 167 (2004) 203–207.
[13] T.S. Zhang, L.B. Kong, Z.Q. Zeng, H.T. Huang, P. Hing, Z.T. Xia, J. Kilner, J. Solid State Electrochem. 7 (2003) 348–354.
[14] C. Kleinlogel, L.J. Gauckler, Solid State Ionics 135 (2000) 567–573.
[15] G.S. Lewis, A. Atkinson, B.C.H. Steele, J. Drennan, Solid State Ionics 152–153 (2002) 567–573.
[16] J.D. Nicholas, L.C. De Jonghe, Solid State Ionics 178 (2007) 1187–1194.
[17] W.Z. Zhu, S.C. Deevi, Mater. Sci. Eng. A 348 (2003) 227–243.
[18] P.L. Lee, D. Shu, M. Ramanathan, C. Preissner, J. Wang, M.A. Beno, R.B. Von Dreele, L. Ribaud, C. Kurtz, S.M. Antao, X. Jiao, B.H. Toby, J. Synchrotron Rad. 15 (2008) 427–432.
[19] A.C. Larson, R.B. Von Dreele, Los Alamos National Laboratory Report LAUR 86-74854 (2004) 55.
[20] B.H. Toby, J. Appl. Cryst. 34 (2001) 210–221.
[21] S. Dikmen, P. Shuka, M. Greenblatt, H. Gocmez, Solid State Sci. 4 (2002) 585–590.
[22] D. Pérez-Coll, P. Núñez, J.C.C. Abrantes, D.P. Fagg, V.V. Kharton, J.R. Frade, Solid State Ionics 176 (2005) 2799–2805.
[23] T.S. Zhang, J. Ma, S.H. Chan, J.A. Kilner, Solid State Ionics 176 (2005) 377–384.
[24] T.S. Zhang, J. Ma, S.H. Chan, P. Hing, J.A. Kilner, Solid State Sci. 6 (2004) 565–572.